



HAL
open science

Synchrotron X-ray interlaced microbeams suppress paroxysmal oscillations in neuronal networks initiating generalized epilepsy.

Benoît Pouyatos, Raphaël Serduc, Mathilde Chipaux, Tanguy Chabrol, Elke Bräuer-Krisch, Christian Nemoz, Hervé Mathieu, Olivier David, Luc Renaud, Yolanda Prezado, et al.

► To cite this version:

Benoît Pouyatos, Raphaël Serduc, Mathilde Chipaux, Tanguy Chabrol, Elke Bräuer-Krisch, et al.. Synchrotron X-ray interlaced microbeams suppress paroxysmal oscillations in neuronal networks initiating generalized epilepsy.. *Neurobiology of Disease*, 2013, 51, pp.152-60. 10.1016/j.nbd.2012.11.005 . inserm-00794543

HAL Id: inserm-00794543

<https://inserm.hal.science/inserm-00794543>

Submitted on 26 Feb 2013

HAL is a multi-disciplinary open access archive for the deposit and dissemination of scientific research documents, whether they are published or not. The documents may come from teaching and research institutions in France or abroad, or from public or private research centers.

L'archive ouverte pluridisciplinaire **HAL**, est destinée au dépôt et à la diffusion de documents scientifiques de niveau recherche, publiés ou non, émanant des établissements d'enseignement et de recherche français ou étrangers, des laboratoires publics ou privés.

Synchrotron x-ray interlaced microbeams suppress paroxysmal oscillations in neuronal networks initiating
generalized epilepsy

Benoît Pouyatos, PhD^{1}, Raphaël Serduc, PhD¹, Mathilde Chipaux, MD, PhD^{2,3}, Tanguy Chabrol¹, Elke Bräuer-Krisch, PhD⁴, Christian Nemoz, PhD⁴, Hervé Mathieu, PhD¹, Olivier David, PhD¹, Luc Renaud⁵, Yolanda Prezado, PhD⁴, Jean-Albert Laissue, MD, PhD⁶, François Estève, MD, PhD¹, Stéphane Charpier, PhD³ and Antoine Depaulis, PhD^{1,2}*

¹ Grenoble Institut des Neurosciences - Inserm U836, Université Joseph Fourier, Grenoble, France.

² Service de Neurochirurgie pédiatrique, Fondation Rothschild, Paris, France.

³ Centre de Recherche de l'Institut du Cerveau et de la Moelle épinière, UPMC/INSERM, UMR-S 975; CNRS UMR 7225, Paris, France.

⁴ European Synchrotron Research Facility, Biomedical beamline ID17, Grenoble, France.

⁵ Centre de Recherche Cerveau et Cognition, CNRS UMR 5549, Toulouse, France.

⁶ Institute of Pathology, University of Bern, Switzerland

Corresponding author:

Benoît Pouyatos, PhD

Grenoble Institut des Neurosciences, Inserm U836, Equipe 11

Bâtiment Edmond J. Safra

Chemin Fortuné Ferrini

38700 La Tronche

Tel +33(0)456520624

Cell +33(0)650041820.

Fax +33(0)456520598

bpouyatos@gmail.com

Keywords: Epilepsy; Animal model; Spike-Wave discharges; Radiotherapy; Synchrotron x-ray microbeams; intracellular recordings; in vivo

Abbreviations:

S1Cx: Primary Somatosensory Cortex;

MoCx: Primary Motor Cortex;

VLTN: Ventrolateral Thalamic Nuclei;

GAERS: Genetic Absence Epilepsy Rat from Strasbourg;

IntMRT: Interlaced Microbeam Radiation Therapy;

MB: Microbeam;

SWDs: Spike-Wave Discharges;

LFPs: Local Field Potentials;

EEG: Electroencephalogram;

MRI: Magnetic Resonance Imaging.

Highlights:

- We developed a radiotherapeutic method using synchrotron x-ray microbeams
- We recorded intracellular activity of irradiated cortical neurons in epileptic rats.
- Irradiation decreased neuronal excitability, reduced propagated synaptic activities
- Paroxysmal oscillations were suppressed in the irradiated tissue.

MODIFICATIONS IN THE TEXT ARE HIGHLIGHTED IN GRAY

ABSTRACT

Radiotherapy has shown some efficacy for epilepsies but the insufficient confinement of the radiation dose to the pathological target reduces its indications. Synchrotron-generated x-rays overcome this limitation and allow the delivery of focalized radiation doses to discrete brain volumes *via* interlaced arrays of microbeams (IntMRT). Here, we used IntMRT to target brain structures involved in seizure generation in a rat model of absence epilepsy (GAERS). We addressed the issue of whether and how synchrotron radiotherapeutic treatment suppresses epileptic activities in neuronal networks. IntMRT was used to target the somatosensory cortex (S1Cx), a region involved in seizure generation in the GAERS. The antiepileptic mechanisms were investigated by recording multisite local-field potentials and the intracellular activity of irradiated S1Cx pyramidal neurons *in vivo*. MRI and histopathological images displayed precise and sharp dose deposition and revealed no impairment of surrounding tissues. Local-field potentials from behaving animals demonstrated a quasi-total abolition of epileptiform activities within the target. The irradiated S1Cx was unable to initiate seizures, whereas neighboring non-irradiated cortical and thalamic regions could still produce pathological oscillations. *In vivo* intracellular recordings showed that irradiated pyramidal neurons were strongly hyperpolarized, displayed a decreased excitability and a reduction of spontaneous synaptic activities. These functional alterations explain the suppression of large-scale synchronization within irradiated cortical networks. Our work provides the first post-irradiation electrophysiological recordings of individual neurons. Altogether, our data are a critical step towards understanding how X-ray radiation impacts neuronal physiology and epileptogenic processes.

INTRODUCTION

Synchrotron X-ray sources have been used for different medical applications among which brain radiosurgery appears as one of the most promising (Dilmanian et al., 2006). By taking benefit of the synchrotron beam's unique properties (high flux of photons, negligible divergence and a lateral dose-off about 200 times steeper than conventional radiotherapy), it is possible to shape quasi-parallel 25-50- μm -thick microbeams (MBs) that can deliver high-doses of radiation deep in the brain within short exposure times (Anschel et al., 2010; Serduc et al., 2010a). These arrays of MBs are surprisingly well tolerated by brain tissue, especially by the vascular system, which is very sensitive to ionizing radiation (Serduc et al., 2006). By interlacing these MBs (Fig 1A; Movie S1), it is possible to deposit high doses of radiation into discrete regions of rat brains, with almost no incidence on the neighboring tissue (Serduc et al., 2010b) (Fig 1B,C and E). We called this new method *Interlaced Microbeam Radiotherapy* (IntMRT). The submillimetric precision of targeting combined to the preservation of surrounding tissue makes IntMRT clinically attractive for all pathologies that require circumscribed destruction and/or inactivation of small brain regions, even if close to eloquent or vital structures.

Until now, IntMRT has been applied to brain tumors (Bouchet et al., 2010; Serduc et al., 2010b) but other non-cancerous pathologies, such as epilepsy, might benefit from the use of synchrotron MBs. Indeed, epileptic seizures generally arise from restricted brain volumes that can often be identified by non-invasive methods, but surgical resection, although very effective (Engel, 1996; Kahane, 2004), cannot always be performed. Radiotherapeutic irradiation of epileptic foci using conventional clinical devices, such as Gamma-Knife®, Cyberknife® or Linacs, has shown some efficacy, but the lateral dose fall-off (Fig 1B) is often insufficient to deposit adequate doses in the target when sensitive/eloquent structures are adjacent (Sims et al., 1999; St George et al., 2002). Given its unique precision (Serduc et al., 2010b), IntMRT may overcome these limitations.

Several studies in patients (Prayson and Yoder, 2007; Rheims et al., 2011) and animals models (Maesawa et al., 2000; Mori et al., 2000; Chen et al., 2001) suggest that an antiepileptic effect may be obtained after irradiation even when the structure targeted is not necrotized. This non-destructive radiotherapeutic effect could be partly caused by biochemical alterations and neuromodulation, yet the cellular mechanisms remain elusive (Rheims et al., 2011; Quigg et al., 2012). Here, we took advantage of the sharp dose fall-off of IntMRT to investigate the functional effects of X-ray radiation on ictogenic neurons, and the result of their inactivation on the seizure onset and its propagation. One of the prerequisite for such experiments was to target an epileptic tissue with well-identified ictogenic neurons, and no cell loss and/or sclerosis to facilitate the assessment of radiation-induced changes. For these reasons and because it allows both long term seizure monitoring and access to the ictal activity of individual neurons (Polack et al., 2007), we chose to perform IntMRT in the Genetic Absence Epilepsy Rats from Strasbourg (GAERS), a strain that displays spontaneous spike-wave discharges (SWDs) reminiscent of human absence seizures (Danober et al., 1998). We targeted bilaterally the so-called “cortical focus”, i.e. the somatosensory cortex (S1Cx; Fig 1C,D), as well as two structures involved in the propagation and maintenance of SWDs (Fig S1), i.e. the motor cortex (MoCx) and the ventro-lateral thalamic nuclei (VLTN). In each animal, we verified the correct targeting by T1-weighted magnetic resonance within the two weeks that followed IntMRT and examined their general behavior by standard tests to detect possible side effects. During the 4 months following irradiation, we monitored weekly the seizures in freely moving animals by recording local-field potentials (LFPs) from depth electrodes implanted in the three target regions. Finally, we investigated the mechanisms underlying the antiepileptic effect by performing *in vivo* intracellular recordings of individual irradiated neurons of the S1Cx.

MATERIAL AND METHODS

Animals.

Fourteen adult female GAERS were bilaterally irradiated in the S1Cx, 3 in the MoCx and 11 in the VLTN. Two S1Cx-irradiated rats were used for intracellular recordings. Twenty-eight GAERS were non-irradiated controls, including 14 for intracellular recordings. We performed all experiments in accordance with the Directive 86/609/EEC after validation by our local ethical committee.

Beam alignment and IntMRT

Microbeam radiation therapy was performed at the ID17 biomedical beamline at the European Synchrotron Radiation Facility (Grenoble, France). For microbeam exposures, a wiggler gap of 24.8 mm was used to produce a white spectrum of photons that extends after filtration (Be (0.5 mm), C (1.5 mm), Al (1.5 mm) and Cu (1.0 mm)) from 50 to 350 keV (mean energy of 90 keV) (Brauer-Krisch et al., 2003). The dose rate was approximately $16,000 \text{ Gy}\cdot\text{s}^{-1}$. For the imaging/alignment of the animals, a high gap aperture (120 mm) was applied to reduce the photons flux by a factor of 6.103 and the energy spectrum to 35-60 keV. These irradiation and imaging methods are described elsewhere (Serduc et al., 2010a,b). Briefly, anaesthetized GAERS rats were prone positioned on a y-axis rotation stage installed above the Kappa-type goniometer (Huber, Germany) and approximately aligned in the beam. Ten, 1-mm thick, x-ray projections of the rat head were acquired with a 1 mm step on a FReloN detector and the reconstructed image was used to define the irradiation fields. The bregma was visualized on the X-ray image and taken as the reference point. The coordinates of the irradiation targets are shown in Fig. 1D. Then, the quasi-laminar beam was spatially fractionated into an array of microbeams (50 μm wide, 200 μm on-center distance) by driving the multislit collimator into the beam. The wiggler gap was closed to 24.8 mm and each epileptic focus was irradiated using 4 irradiation ports separated by a 45° angle and a 50 μm step, both applied in the y-axis to generate a solid dose deposition at the interlaced region. The MB entrance dose (200 Gy) was chosen based on

the immunohistological results presented in Serduc et al., 2010b. At this dose, the tissue integrity was maintained, but exhibited numerous cell deaths 30 days post-irradiation. We assessed volumic dose in a rat head phantom for each target (Fig 1B) by using PENELOPE-2006 Monte Carlo code (Salvat and Fernández-Varea, 2006; Prezado et al., 2009). We calculated the ratios between the valley doses within and outside the interlaced targets (Fig 1D).

Behavioral tests.

Two weeks after IntMRT, we estimated sensorimotor coordination using an accelerating paradigm (4-40 rpm, 5 min) on the Rotarod[®] (Panlab/Harvard Apparatus) by averaging the latencies to fall off the rotating rod (3 trials). The same day, rats were placed in the center of an open-field arena for 20 min and locomotion was video-tracked and quantified.

Magnetic resonance (MR) imaging

Two weeks after IntMRT, we obtained 7T-MRI (Bruker Biospec Avance III) in all rats. We characterized brain vessel permeability using a T1w sequence (TurboRARE. TR: 1300 ms, effective TE: 7.7 ms, FOV: 30x30 mm, matrix: 256x256, slice thickness: 0.5 mm) acquired ~5 min after intravenous injection of Gadolinium (200 mmol.kg⁻¹, Dotarem, Guerbet).

LFP monitoring in freely moving rats

Sixteen days post-irradiation, we implanted rats with two supra-dural screws (fronto-parietal) and three bipolar depth electrodes in the right S1Cx, MoCx and VLTN (same coordinates as the centers of the irradiation targets specified in Fig 1D). We monitored LFPs weekly (1 h) from the 4th to the 16th post-irradiation week using System-Plus Evolution[®] (Micromed) and quantified SWDs. At 8 weeks post-irradiation, we acquired LFPs with high-sampling rate (5 kHz) on 2-3 rats/group for qualitative assessment of SWD characteristics using a headstage preamplifier (MPA8I; Multi Channel Systems) connected to a multichannel amplifier (FA32I; Multi Channel Systems) and to Power 1401 mkII data acquisition device (Cambridge Electronic Design). Seizures were

automatically detected by filtering EEG power in all channels between 6-9 Hz and correcting baseline for mean and standard deviation estimated from the 2 s preceding SWDs. We extracted local maxima of baseline-corrected filtered EEG, and defined seizure onset/termination as the first/last local maximum with amplitude above 6. This procedure was repeated for each electrode in order to calculate delays of propagation of SWDs. For each SWD, we obtained the power of oscillatory activity between 1 and 50 Hz using Morlet wavelet transform. We normalized Time-Frequency maps by subtracting the mean of the baseline to the data, and dividing demeaned data by the standard deviation of the baseline. The degree of statistical ($P < 0.001$) association between LFPs from the S1Cx, MoCx and VLTN bipolar electrodes was determined by calculating the mean nonlinear correlation coefficient h^2 (Lopes da Silva et al., 1989; Wendling et al., 2009) between each pair of electrodes during the first 2 s of representative SWDs ($n = 17-30$). The directionality of the dependence between two electrodes a and b was obtained by calculating the difference between $h^2_{a>b}$ and $h^2_{b>a}$.

In vivo intracellular recordings

We obtained *in vivo* intracellular recordings from non-irradiated ($n = 14$) and S1Cx-irradiated GAERS ($n = 2$) two months following irradiation. Rats were initially anesthetized with sodium pentobarbital and ketamine (40/100 mg.kg⁻¹), then maintained by additional doses of fentanyl, as previously described (Polack et al., 2007). We obtained cortical local field potentials (LFPs) using two low-impedance silver electrodes placed on the *dura* above the S1Cx and MoCx. Intracellular recordings were performed using glass micropipettes filled with 2 M potassium acetate (50–70 M Ω). Membrane input resistance was measured from the linear portion of the voltage-current relationships, which were constructed by the mean ($n = 10-20$) membrane potential changes induced by a wide range (-0.2 to -1 nA) of hyperpolarizing current pulses. The membrane time-constant was the time taken for a -0.4 nA-induced membrane potential deflection to reach 63% of its final value.

Amplitude fluctuations of background membrane potentials were quantified by their standard deviation computed from subthreshold spontaneous activities of 10s duration. We recorded S1Cx cells at 0.1/1.7 mm posterior, 5/6 mm lateral from the bregma, and 0.9/3.3 mm under the cortical surface. Intracellular recordings were obtained under current-clamp using the active bridge mode of an Axoclamp-2B amplifier (Molecular Devices). Data were digitized using Spike 2 (Cambridge Electronic Design) at 10 kHz (intracellular signal) or 1 kHz (EEG). Action potentials were characterized as previously described (Polack et al., 2007). Cross-correlograms between intracellular activities and LFPs were calculated using Spike 2 (Cambridge Electronic Design).

Statistical analyses

Characteristics of intracellular recordings were analyzed using Mann-Whitney tests. Seizure number and durations were analyzed using 2-way repeated-measure ANOVAs, with Bonferroni's post-tests. $P = 0.05$ was considered as the significance threshold. All values are given as mean \pm SEM.

Histopathological analyses.

Short-term histochemical evaluation of irradiation was performed two months post-irradiation by myelin staining using a modified gallyas silver impregnation. We used a classic Nissl staining for visualization of cellular body damage.

RESULTS

IntMRT allows high-precision dose delivery in restricted brain regions with minimal behavioral side effects

MRI acquired 14 days after bilateral S1Cx, MoCx or VLTN (Figs 1C,D and S1) irradiations showed strong, sharply delimited, hypersignals in the regions where MBs interlaced, suggesting an alteration of the vascular integrity and micro-ruptures of the blood-brain barrier within the targets. These images denote a precise targeting and an effective sparing of tissue irradiated with non-interlaced MBs. Two months after IntMRT, we observed no major histological damage outside the interlaced targets, including the regions traversed by a single array of MBs. Occasionally, the tracks of individual MBs appeared on Nissl-stained sections (Fig 1E *left panels*; arrowheads) as thin clear stripes spaced $\approx 200 \mu\text{m}$ apart. At low magnification, Nissl staining appeared heterogeneous in the S1Cx region, reflecting a variable decrease in cell density. On high-magnification images, neurons were often damaged with signs of cell death (white arrow) and neuronophagia (*). After IntMRT, myelin sheaths (*right panels*) appeared fragmented, focally forming argyrophilic fragments (>) and myelin ovoids (#). Myelin fiber structures lost their anisotropy after irradiation and displayed “honeycombing” figures. This histological pattern was in agreement with our previous observations (Serduc et al., 2010b). We did not detect any significant deleterious effect of irradiation on sensorimotor behavior in any of the three irradiated groups, as compared to the non-irradiated animals (Fig S2).

S1Cx bilateral IntMRT irradiation induces a decrease of cumulated seizure duration

Freely-moving LFP monitoring was performed until the 16th week post-irradiation in GAERS implanted with depth electrodes in the S1Cx, MoCx and VLTN. Control GAERS displayed SWDs

arising abruptly from normal EEG background on all channels with an average of 74.4 ± 2.2 SWD/h lasting 18.1 ± 0.35 s (Fig 2A; 204 h of recording, 13,230 SWDs). Four weeks after treatment, animals bilaterally irradiated in the S1Cx displayed SWDs 48% shorter than those of non-irradiated animals ($P < 0.001$), although their number remained approximately the same. This effect, which persisted until the end of the monitoring period, resulted in a significantly reduced cumulated seizure duration in animals irradiated in the S1Cx compared to control animals (grand mean: 12.9 ± 0.53 vs. 22.3 ± 0.70 min/h, respectively; $P < 0.01$). Irradiation of the VLTN also induced a long-lasting reduction of the average SWD duration ($P < 0.001$), but significantly increased their number ($P < 0.001$), which resulted in a cumulated seizure duration similar to controls ($P > 0.05$). Bilateral IntMRT Irradiation of the MoCx did not induce any significant change in seizure number ($P > 0.05$) nor duration ($P > 0.05$).

IntMRT prevents epileptic activities in the targeted regions

In non-irradiated animals, SWDs were characterized by a 25-50-fold increase of the power in the 6-9 Hz frequency band on all channels compared to interictal periods (Fig 2B,C). The bilateral delivery of 200 Gy in any of the three brain targets resulted in a near complete abolition of SWDs on the LFPs recorded from these structures (Fig 2B,C). The average power in the 6-9 Hz frequency band was decreased by 93, 74 and 88% in the irradiated S1Cx, MoCx and VLTN, respectively, when compared to LFP signals recorded from homologous structures in non-irradiated animals (Fig 2C). The strongly altered SWDs recorded in the irradiated structures will be then referred as “residual paroxysmal oscillations” (RPOs). We also observed that the irradiated targets were unable to initiate/lead SWDs, as shown by the delays of propagation of SWDs (Fig S3A) and the non-linear interdependence (h_2 ; Fig S3B) between the recorded structures.

Membrane excitability and background synaptic activity are altered in irradiated S1Cx pyramidal neurons

Recorded neurons located in the infra-granular layers of the S1Cx (Fig 3B, right *inset*) exhibited the intrinsic firing patterns (regular spiking or intrinsic bursting) (Fig 3D,E) and action potential properties (Fig 3D, *inset*) of pyramidal cells. These neurons belong to the neuronal population previously identified as the trigger for SWDs in GAERS (Polack et al., 2007; 2009). Non-irradiated S1Cx neurons ($n = 19$) displayed large-amplitude synaptic fluctuations between SWDs, corresponding to a mean membrane potential of -60.0 ± 0.9 mV and resulting in a sustained (11.2 ± 1.5 Hz) spontaneous firing (Fig 3A,H). Eight S1Cx neurons were intracellularly recorded two months after IntMRT in two rats. These cells displayed a significant ($P < 0.001$) membrane hyperpolarization (Fig 3C,H) associated with a collapse in the firing rate (Fig 3B,H), 5 out of 8 neurons becoming silent (Fig 3B). These effects were associated with a dramatic decrease in the standard deviation of the background synaptic activity (non-irradiated, 5.2 ± 0.4 mV, $n = 19$ neurons vs. irradiated, 1.6 ± 0.2 mV, $n = 8$; $P < 0.0001$; Fig 3C), which was mainly composed of miniature-like depolarizing events (Fig 3B, left *inset*). The great reduction in the spontaneous firing of irradiated neurons did not result from an alteration in the intrinsic processes of spiking since the amplitude, duration and voltage threshold of action potentials were not significantly modified ($P > 0.05$; Fig 3D, *inset*).

IntMRT had a complex effect on membrane excitability. We found a significant attenuation in the neuronal input-output relation, as evidenced by the reduced firing rate in response to +0.4nA current pulses (non-irradiated cells, 45.4 ± 8.6 Hz, $n = 11$ neurons vs. irradiated, 22.4 ± 7.0 Hz, $n = 5$; $P < 0.05$; Fig 3D,E). These effects likely resulted from the membrane hyperpolarization rather than from a diminution of the membrane input resistance since this excitability parameter, measured by the slope of the linear voltage-current relationship (Fig 3F,G), was significantly increased in irradiated

neurons ($P < 0.05$; Fig 3H). In contrast, the passive membrane time constant, which defined the temporal window over which synaptic potentials can sum (Rall, 1969; Spruston et al., 2007), was significantly decreased ($P < 0.05$; Fig 3E *inset* and H).

The antiepileptic effect of IntMRT is associated with a lack of synchronized neuronal oscillations in the S1Cx

We further explored the cellular mechanisms of IntMRT by comparing the intracellular activities of irradiated S1Cx cells during RPOs with those occurring during SWDs in non-irradiated GAERS. In control cells, we recorded oscillatory suprathreshold depolarizations (Fig 4A,C) superimposed on a sustained membrane hyperpolarization (-4.6 ± 0.8 mV) lasting for the entire duration of the SWD (Fig 4A). As indicated by the strong cross-correlation between the LFP and intracellular waveforms (Fig 4C), SWDs resulted from synchronized spatiotemporal oscillations in the underlying cortical synaptic network. This rhythmic activity was completely disrupted by IntMRT since only short periods of RPOs persisted in the LFP recordings (Fig 4B). Concomitantly, the membrane potential was significantly more hyperpolarized in irradiated neurons than in control neurons during SWDs ($P < 0.05$; Fig 4B,F). During RPOs, most irradiated neurons remained silent ($n = 6$ neurons), but summation of erratic synaptic depolarizations could cause a scattered firing ($n = 2$, Fig 4B,E Irradiated). Rare synchronized activities recorded in “non-silent” neurons were likely at the origin of the occasional RPOs at the cortical surface. The cross-correlation between intracellular activities of irradiated S1Cx cells and RPOs indicated a weak temporal coherence between the two signals (Fig 4D) and suggested a reduced synchronization among cortical cells.

Altogether, our *in vivo* intracellular recordings of S1Cx irradiated neurons demonstrated a global decrease in the membrane excitability, along with a spatiotemporal disorganization of the ongoing

synaptic activity and the disappearance of synchronized oscillations. These coherent/synergistic changes likely explain the local suppression of SWDs.

DISCUSSION

In the GAERS model of generalized epilepsy, we applied a novel method of radiotherapy utilizing the unique properties of synchrotron X-ray MBs. We took advantage of the excellent precision and sharp lateral dose gradient provided by the IntMRT geometry to investigate for the first time the post-irradiation activities of ictogenic neurons, and the consequence of their inactivation on global seizure initiation and propagation.

IntMRT reduces the excitability and synchronization of SICx neurons

Our *in vivo* intracellular recordings within the irradiated SICx indicated that the integrative properties and firing output of pyramidal neurons were significantly affected. The concomitant membrane hyperpolarization, the increase in apparent membrane input resistance and the reduction in membrane time constant could partly result from a decrease in the total cell membrane area after irradiation. Indeed, such structural alteration may reduce the number of ion channels available for current to leak through the membrane and decrease the membrane capacitance, therefore accelerating the initial rate of change of trans-membrane voltage. Consistent with this hypothesis, increase in membrane input resistance, decrease in membrane capacitance and cell hyperpolarization have been described in cortical pyramidal neurons after dendrotomy (Bekkers and Häusser, 2007). Our results thus suggest an alteration of neuronal morphology with a reduction of the total membrane surface, as observed in hippocampal pyramidal cells in slices from neonatally irradiated rats (Czéh et al., 1999). However, the increase in the cells' input resistance also indicates that the severed neuronal membrane, possibly caused by a direct effect of ionizing radiations, was able to reseal. The reduction of spontaneous synaptic events in irradiated neurons might also participate in the enhancement of both membrane resistance and polarization (Destexhe and Paré, 1999) as previously described in the GAERS (Polack et al., 2009). It is also conceivable that the concomitant

effects on synaptic and membrane properties could result, at least in part, from the alteration of the cation current I_h since its blockade in epileptic slices decreases the occurrence of spontaneous epileptiform events together with an increase in resting membrane potential and apparent input resistance (Inaba et al., 2006).

Despite these alterations in their passive membrane properties, irradiated neurons were still capable to fire action potentials similar to those of homologous neurons in non-irradiated rats. This is consistent with the persistence of high-frequency, current-evoked, neuronal discharges in cortical slices from irradiated rats (Zhou et al., 2009). However, in our study, the responsiveness of irradiated cells for a given stimulus was substantially attenuated, indicating a global decrease in their intrinsic excitability that was mainly due to the membrane hyperpolarization. The spontaneous activity of irradiated S1Cx cells is also considerably dampened in-between and during the RPOs. In particular, the depolarizing background synaptic activities were diminished in amplitude and frequency, a finding in accordance with the reduced rate of excitatory synaptic events found in irradiated neocortical networks (Xiang et al., 2006). Here, the decline in the excitatory synaptic drive of irradiated S1Cx was likely due to a partial loss of local excitatory neurons and to an alteration of axonal myelination affecting the propagation of synaptic activities. These structural changes together with the membrane hyperpolarization and the shorter membrane time constant were likely responsible for the low spontaneous firing and the lack of paroxysmal depolarizing shifts. Consequently, this may have precluded the synchronization among cortical cells and the generation of fully developed SWDs.

IntMRT: a unique tool to investigate the focal effects of x-ray radiation.

A review of the literature reveals that the *focal* antiepileptic mechanisms of radiations were extremely difficult - if not impossible - to investigate in rodent models of epilepsy because of the insufficient confinement of the dose provided by megavoltage clinical devices (Maesawa et al.,

2000; Chen et al., 2001; Brisman et al., 2003; Jenrow et al., 2004). By contrast, IntMRT allowed the specific irradiation of discrete brain regions and the assessment of both the functional changes within the target, and the effect of its irradiation on seizure dynamics at the brain scale. For instance, we obtained a reduction of the cumulated seizure duration only when the S1Cx was bilaterally irradiated. This effect was specific to this target and was not observed when either the MoCx or the VLTN were irradiated. This result is in agreement with the anti-absence effect of ethosuximide when injected in the S1Cx, but not in the MoCx in GAERS (Manning et al., 2004). We also observed that the irradiation of the S1Cx did not prevent the MoCx and VLTN from displaying paroxysmal oscillations. We propose that the non-irradiated thalamocortical networks were able to initiate SWDs, although with a lesser efficacy. By contrast, the bilateral thalamic irradiation left both the S1Cx and the MoCx free to oscillate in synchrony without thalamic feedback control, which would explain the increase of the number of SWDs.

Clinical potential of synchrotron X-ray microbeams

During the last two decades, radiosurgery has emerged as an attractive approach for epilepsy treatment and several clinical studies using mainly Gamma-Knife® and linear accelerators reported acceptable outcomes for hypothalamic hamartomas, arteriovenous malformations and cavernomas (Romanelli and Anschel, 2006; Quigg et al., 2012). By contrast, for epilepsies arising from the mesio-temporal lobe, several reports (Schröttner et al., 2002; Régis et al., 2004; Vojtech et al., 2009) suggest that efficacy is highly dependent on the dose deposited within the target, which is intrinsically limited by the bell-shaped lateral dose gradients of the current devices. In such clinical context, the synchrotron light provides attractive physical properties in terms of precision and conformation of the dose delivery. In addition, several research groups (*i.e.* LAL in Paris or MAP in Munich) and companies (*i.e.* LynceanTech) have been recently developing compact X-ray

synchrotron sources, which aim at providing a photon flux and spectrum that matches the clinical requirement for imaging and/or radiotherapy. Given that the effect of radiotherapeutic doses of X-rays on brain physiology is largely unknown, there is an important need for experimental studies that investigate the electrophysiological and histological effect of low-energy photons on laboratory animals carrying pathologies. As such, our study represents the first proof of concept in the preclinical evaluation of synchrotron MBs for the treatment of epilepsies. Several fundamental and technical problems still have to be solved before synchrotron microbeams can be considered for clinical development, including the assessment of the IntMRT effect on pharmacoresistant tissue suffering from major cell loss and/or gliosis, and the practical feasibility of irradiations on bigger animals and humans. Indeed, the use of IntMRT on larger targets will require minimizing irradiations of major blood vessels, and a careful choice of dose in order to find a subtle balance between the elimination of epileptic activities and the tolerance of the vascular network to ionizing radiations. Nevertheless, our data clearly show a clinical potential of IntMRT for epilepsy, and highlight a non-destructive antiepileptic mechanism that might be a common effect of both x-ray and gamma radiations on brain tissue.

Conclusions

Together, our results show that IntMRT was able to modify an epileptogenic cortex and disabled its ability to initiate seizures by preventing wide-scale synchronization among irradiated neuronal networks. This effect was mediated through a neuronal membrane hyperpolarization and an alteration of propagated synaptic activities, presumably caused by reduction a total cell membrane area. The present study provides a foundation to understand how x-ray radiation impacts neuronal physiology and epileptogenic processes and opens new perspectives for synchrotron microbeam radiotherapy.

Acknowledgments

We thank H. Bernard, L. Duhamel, T. Ziegenhals and T. Brochard for their technical assistance. We are indebted to C. Deransart, I. Guillemain, S. Carnicella and A. Bravin for their valuable scientific advices and access to equipment, as well as to J. Crosbie and L. Fechter for comments on a previous version of the manuscript. **Funding:** This work was supported by Institut National de la Santé et de la Recherche Médicale, Agence Nationale pour la Recherche (Grant #ANR RO6275CS “BasalEpi”), Ligue Française Contre l’Epilepsie and European Synchrotron Research Facility. **Author contributions:** B.P., R.S., F.E. and A.D designed the research. B.P., R.S., M.C., T.C., E.B.K., C.N., H.M., L.R., Y.P., S.C., J.A.L and A.D performed the research. B.P., M.C., T.C, L.R., J.A.L, S.C. and A.D analyzed the data. B.P., R.S., M.C., S.C., A.D, J.A.L and F.E. wrote the paper **Competing interests:** The authors declare that there are no conflicts of interest.

REFERENCES

- Anschel, D.J., Bravin, A., Romanelli, P., 2010. Microbeam radiosurgery using synchrotron-generated submillimetric beams: a new tool for the treatment of brain disorders. *Neurosurg Rev* 34, 133–142.
- Bekkers, J.M., Häusser, M., 2007. Targeted dendrotomy reveals active and passive contributions of the dendritic tree to synaptic integration and neuronal output. *Proc Natl Acad Sci USA* 104, 11447–11452.
- Bouchet, A., Lemasson, B., Le Duc, G., Maisin, C., Bräuer-Krisch, E., Siegbahn, E.A., Renaud, L., Khalil, E., Rémy, C., Poillot, C., Bravin, A., Laissue, J.A., Barbier, E.L., Serduc, R., 2010. Preferential effect of synchrotron microbeam radiation therapy on intracerebral 9L gliosarcoma vascular networks. *Int J Radiat Oncol Biol Phys* 78, 1503–1512.
- Brauer-Krisch, E., Bravin, A., Lerch, M., Rosenfeld, A., Stepanek, J., Di Michiel, M., Laissue, J.A., 2003. MOSFET dosimetry for microbeam radiation therapy at the European Synchrotron Radiation Facility. *Med Phys* 30, 583–589.
- Brisman, J.L., Cole, A.J., Cosgrove, G.R., Thornton, A.F., Rabinov, J., Bussiere, M., Bradley-Moore, M., Hedley-Whyte, T., Chapman, P.H., 2003. Radiosurgery of the Rat Hippocampus: Magnetic Resonance Imaging, Neurophysiological, Histological, and Behavioral Studies. *Neurosurgery* 951–962.
- Chen, Z., Kamiryo, T., Henson, S., Yamamoto, H., Bertram, E., Schottler, F., Patel, F., Steiner, L., Prasad, D., Kassell, N., 2001. Anticonvulsant effects of gamma surgery in a model of chronic spontaneous limbic epilepsy in rats. *J Neurosurg* 94, 270–280.
- Czéh, B., Seress, L., Czéh, G., 1999. Electrophysiological characteristics and morphological properties of dentate granule--and CA3 pyramidal cells in slices cut from neonatally irradiated rats. *Neurobiology (Bp)* 7, 1–17.
- Danober, L., Deransart, C., Depaulis, A., Vergnes, M., Marescaux, C., 1998. Pathophysiological mechanisms of genetic absence epilepsy in the rat. *Prog. Neurobiol.* 55, 27–57.
- Destexhe, A., Paré, D., 1999. Impact of network activity on the integrative properties of neocortical pyramidal neurons in vivo. *J Neurophysiol* 81, 1531–1547.
- Dilmanian, F.A., Zhong, Z., Bacarian, T., Benveniste, H., Romanelli, P., Wang, R., Welwart, J., Yuasa, T., Rosen, E.M., Anschel, D.J., 2006. Interlaced x-ray microplanar beams: a radiosurgery approach with clinical potential. *Proc Natl Acad Sci USA* 103, 9709–9714.
- Engel, J., 1996. Surgery for seizures. *N Engl J Med* 334, 647–652.
- Inaba, Y., Biagini, G., Avoli, M., 2006. The H current blocker ZD7288 decreases epileptiform hyperexcitability in the rat neocortex by depressing synaptic transmission. *Neuropharmacology* 51, 681–691.
- Jenrow, K., Ratkewicz, A., Lemke, N., Kadiyala, M., Zalinski, D., Burdette, D., Elisevich, K., 2004. Effects of kindling and irradiation on neuronal density in the rat dentate gyrus. *Neurosci Lett* 371, 45–50.
- Kahane, P., 2004. La chirurgie de l'“épilepsie chez l'adulte: pour qui? *Revue Neurologique*.
- Lopes da Silva, F., Pijn, J.P., Boeijinga, P., 1989. Interdependence of EEG signals: linear vs. nonlinear associations and the significance of time delays and phase shifts. *Brain Topogr* 2, 9–18.
- Maesawa, S., Kondziolka, D., Dixon, C.E., Balzer, J., Fellows, W., Lunsford, L.D., 2000. Subnecrotic stereotactic radiosurgery controlling epilepsy produced by kainic acid injection in rats. *J Neurosurg* 93, 1033–1040.
- Manning, J.P.A., Richards, D.A., Leresche, N., Crunelli, V., Bowery, N.G., 2004. Cortical-area

- specific block of genetically determined absence seizures by ethosuximide. *Neuroscience* 123, 5–9.
- Mori, Y., Kondziolka, D., Balzer, J., Fellows, W., Flickinger, J.C., Lunsford, L.D., Thulborn, K.R., 2000. Effects of stereotactic radiosurgery on an animal model of hippocampal epilepsy. *Neurosurgery* 46, 157–65; discussion 165–8.
- Polack, P.-O., Guillemain, I., Hu, E., Deransart, C., Depaulis, A., Charpier, S., 2007. Deep layer somatosensory cortical neurons initiate spike-and-wave discharges in a genetic model of absence seizures. *J Neurosci* 27, 6590–6599.
- Polack, P.-O., Mahon, S., Chavez, M., Charpier, S., 2009. Inactivation of the somatosensory cortex prevents paroxysmal oscillations in cortical and related thalamic neurons in a genetic model of absence epilepsy. *Cereb Cortex* 19, 2078–2091.
- Prayson, R.A., Yoder, B.J., 2007. Clinicopathologic findings in mesial temporal sclerosis treated with gamma knife radiotherapy. *Ann Diagn Pathol* 11, 22–26.
- Prezado, Y., Fois, G., Le Duc, G., Bravin, A., 2009. Gadolinium dose enhancement studies in microbeam radiation therapy. *Med Phys* 36, 3568–3574.
- Quigg, M., Rolston, J., Barbaro, N.M., 2012. Radiosurgery for epilepsy: clinical experience and potential antiepileptic mechanisms. *Epilepsia* 53, 7–15.
- Rall, W., 1969. Time constants and electrotonic length of membrane cylinders and neurons. *Biophys J* 9, 1483–1508.
- Régis, J., Rey, M., Bartolomei, F., Vladyka, V., Liscak, R., Schröttner, O., Pendl, G., 2004. Gamma knife surgery in mesial temporal lobe epilepsy: a prospective multicenter study. *Epilepsia* 45, 504–515.
- Rheims, S., Didelot, A., Guenot, M., Régis, J., Ryvlin, P., 2011. Subcontinuous epileptiform activity after failed hippocampal radiosurgery. *Epilepsia* 52, 1425–1429.
- Romanelli, P., Anschel, D.J., 2006. Radiosurgery for epilepsy. *Lancet Neurol* 5, 613–620.
- Salvat, F., Fernández-Varea, J., 2006. PENELOPE-2006: A code system for Monte Carlo simulation of electron and photon transport. *Workshop Proceedings*.
- Schröttner, O., Unger, F., Eder, H.G., Feichtinger, M., Pendl, G., 2002. Gamma-Knife radiosurgery of mesiotemporal tumour epilepsy observations and long-term results. *Acta Neurochir. Suppl.* 84, 49–55.
- Serduc, R., Berruyer, G., Brochard, T., Renier, M., Nemoz, C., 2010a. In vivo pink-beam imaging and fast alignment procedure for rat brain lesion microbeam radiation therapy. *J Synchrotron Radiat* 17, 325–331.
- Serduc, R., Bräuer-Krisch, E., Siegbahn, E.A., Bouchet, A., Pouyatos, B., Carron, R., Pannetier, N., Renaud, L., Berruyer, G., Nemoz, C., Brochard, T., Rémy, C., Barbier, E.L., Bravin, A., Le Duc, G., Depaulis, A., Estève, F., Laissue, J.A., 2010b. High-precision radiosurgical dose delivery by interlaced microbeam arrays of high-flux low-energy synchrotron X-rays. *PLoS ONE* 5, e9028.
- Serduc, R., Vérant, P., Vial, J.-C., Farion, R., Rocas, L., Rémy, C., Fadlallah, T., Brauer, E., Bravin, A., Laissue, J., Blattmann, H., van der Sanden, B., 2006. In vivo two-photon microscopy study of short-term effects of microbeam irradiation on normal mouse brain microvasculature. *Int J Radiat Oncol Biol Phys* 64, 1519–1527.
- Sims, E., Doughty, D., Macaulay, E., Royle, N., Wraith, C., Darlison, R., Plowman, P.N., 1999. Stereotactically delivered cranial radiation therapy: a ten-year experience of linac-based radiosurgery in the UK. *Clin Oncol (R Coll Radiol)* 11, 303–320.
- Spruston, N., Stuart, G., Häusser, M., 2007. Dendrites, in: Stuart, G., Spruston, N. (Eds.), *Dendrites*. Oxford University Press, USA, pp. 351–400.
- St George, E.J., Kudhail, J., Perks, J., Plowman, P.N., 2002. Acute symptoms after gamma knife

- radiosurgery. *J Neurosurg* 97, 631–634.
- Vojtech, Z., Vladyka, V., Kalina, M., Nespore, E., Seltenreichová, K., Semnická, J., Liscak, R., 2009. The use of radiosurgery for the treatment of mesial temporal lobe epilepsy and long-term results. *Epilepsia* 50, 2061–2071.
- Wendling, F., Ansari-Asl, K., Bartolomei, F., Senhadji, L., 2009. From EEG signals to brain connectivity: a model-based evaluation of interdependence measures. *J Neurosci Methods* 183, 9–18.
- Xiang, H., Chen, H.-X., Yu, X.-X., King, M.A., Roper, S.N., 2006. Reduced excitatory drive in interneurons in an animal model of cortical dysplasia. *J Neurophysiol* 96, 569–578.
- Zhou, F.-W., Chen, H.-X., Roper, S.N., 2009. Balance of inhibitory and excitatory synaptic activity is altered in fast-spiking interneurons in experimental cortical dysplasia. *J Neurophysiol* 102, 2514–2525.

FIGURES

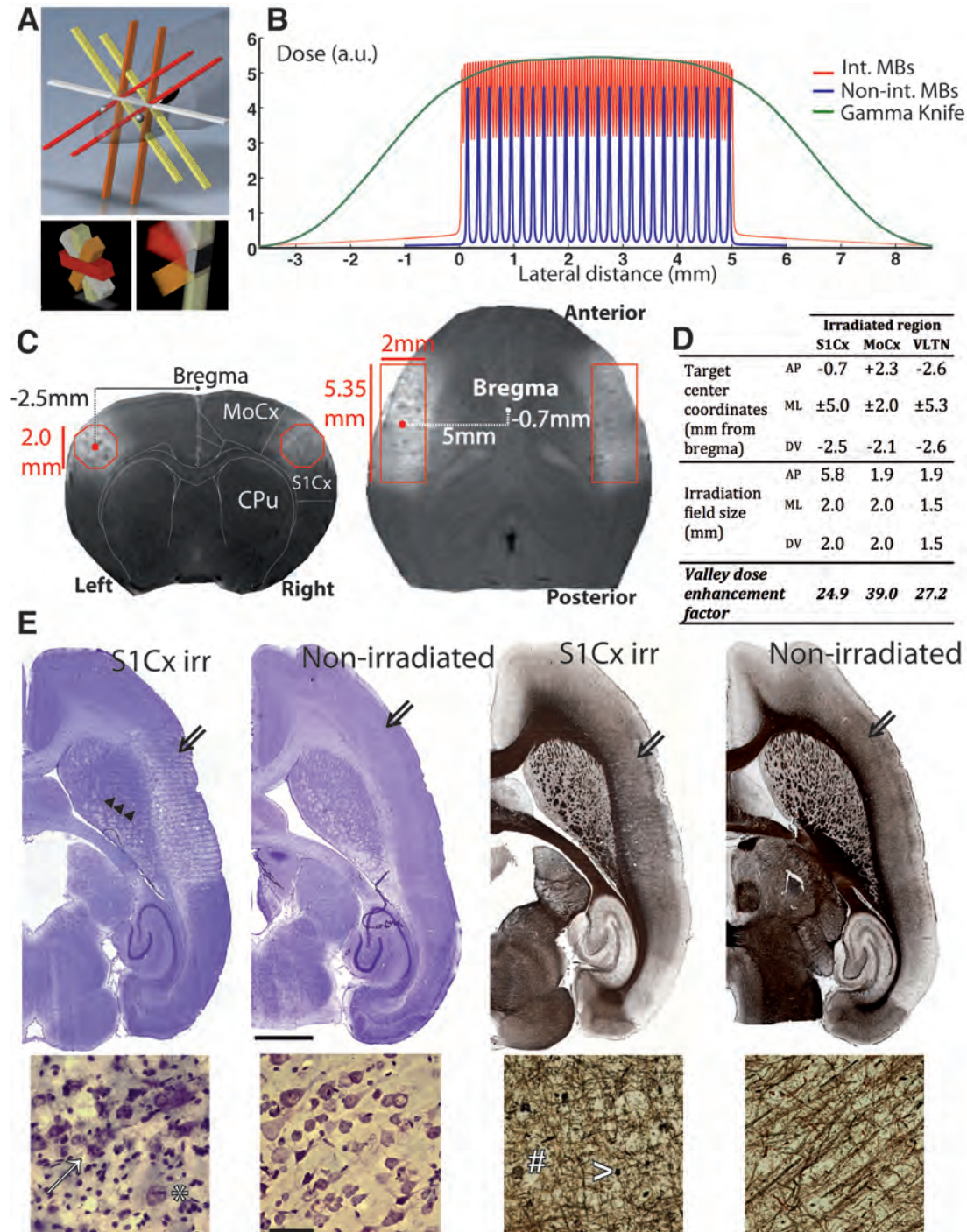
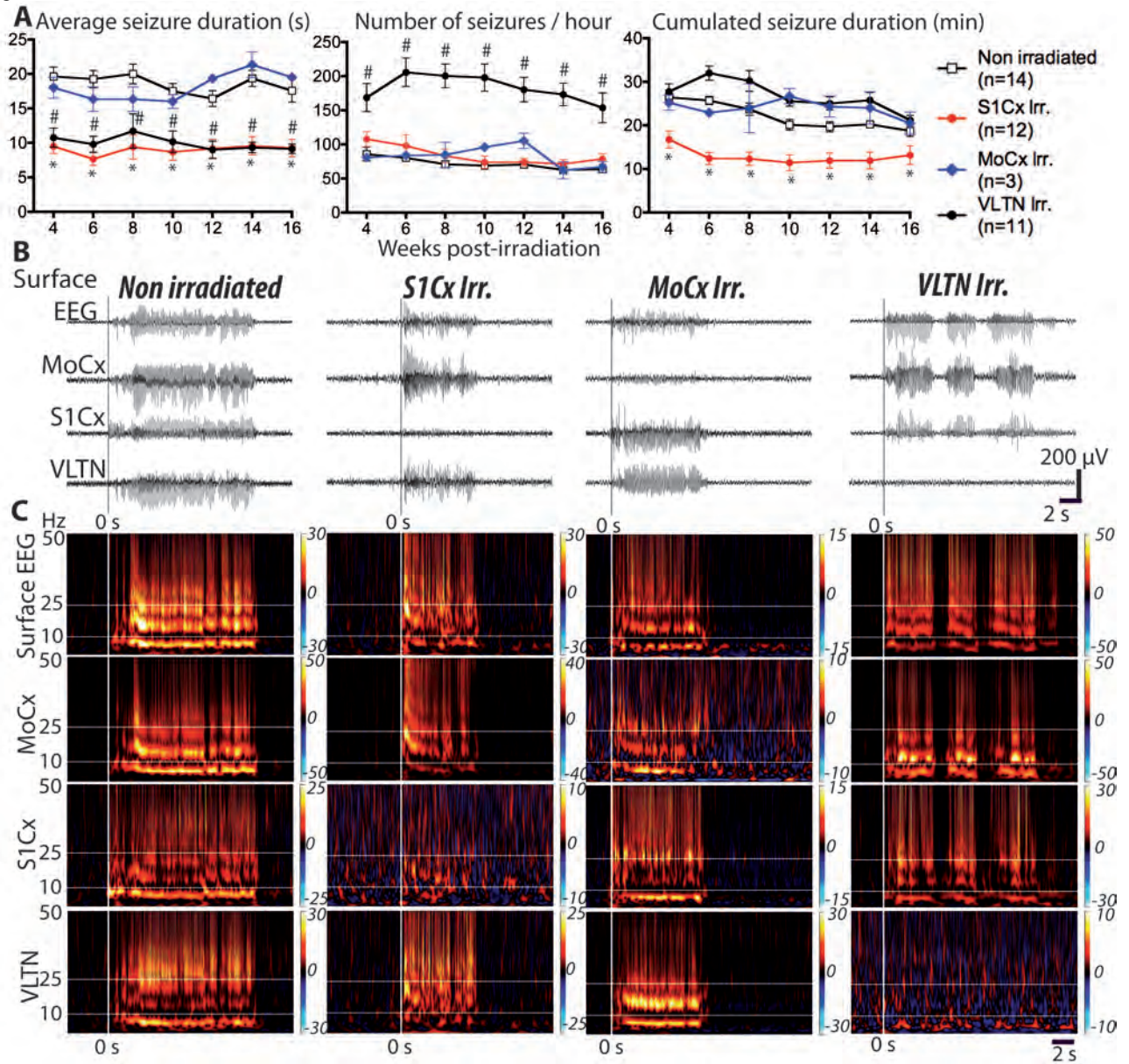


Figure 1.

Irradiation geometry, magnetic resonance imaging and histopathological changes. (A) Diagram of the 4-port MB interlacement for bilateral S1Cx irradiation. The region receiving a homogenous dose is displayed in gray. (B) Lateral dose-profiles for a 5mm-wide irradiation field produced by interlaced and non-interlaced MBs and by a Leksell Perfexion® Gamma-Knife. (C) Theoretical delimitations of homogeneously irradiated volumes superimposed on horizontal and coronal T1w/GdDOTA-MR images acquired 14 days post-irradiation (200 Gy). CPu: caudate-putamen. (D) Coordinates of the three experimental targets. Valley dose enhancement factors, calculated with Monte-Carlo

simulations, correspond to the valley-dose ratio between the center of the target and 1 mm away from the target. **(E)** Microphotographs of horizontal brain sections obtained 2 months post-irradiation compared to sections from non-irradiated brains. Sections were stained by the Nissl method (4 left panels) and for myelin sheaths (4 right panels). Lower-magnification photographs of the irradiated brain show decreases of Nissl and myelin staining densities in the S1Cx. Tracks of individual 200 μ m-spaced MBs outside the target are visible in the striatum (arrowheads). Double-arrows indicate the area where high-magnification photographs were captured. Signs of neuronal damage are visible on the Nissl-stained section: rounded shapes, vacuolation (clear arrow), nuclear debris and accumulation of microglial cells around damaged neurons (*, neuronophagia). Myelin staining shows radiation-induced fragmentation of myelin sheaths, focally forming argyrophilic fragments (>) and few myelin ovoids (#). Irradiated tissue displays typical “honeycombing” figures. Scale bars: 2mm (lower-magnification images) and 100 μ m (high-magnification images).

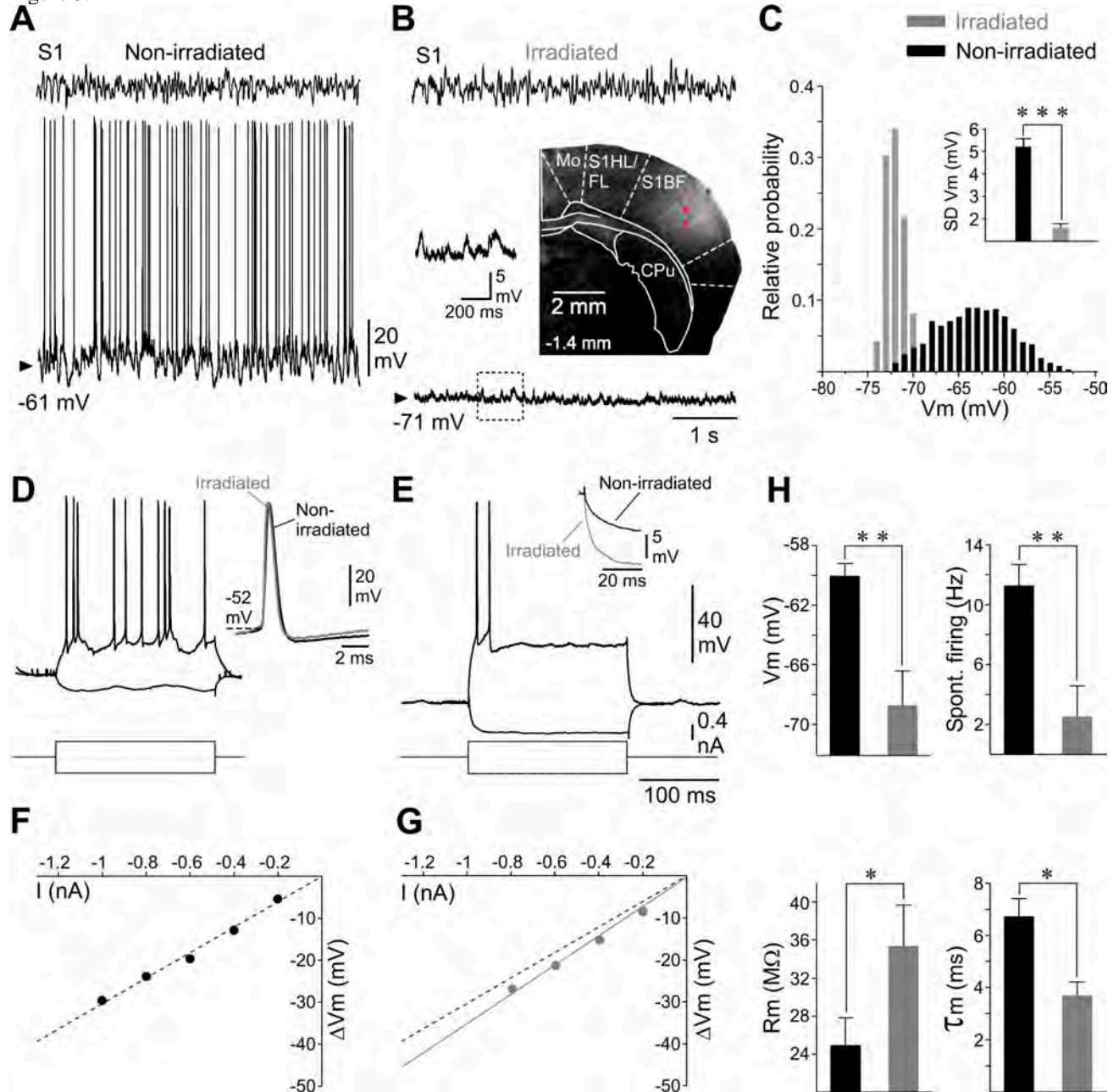
Figure 2.



Spike-wave discharges after IntMRT irradiation. (A) EEG monitoring of average seizure duration, number of seizures per hour and cumulated seizure time. * and #: S1Cx- and VLTN-irradiated groups differ significantly from non-

irradiated animals, respectively ($P < 0.05$). For sake of clarity, only the data obtained every two weeks are shown here. **(B)** Examples of typical seizures recorded in the non-irradiated, S1Cx-, MoCx- and VLTN-irradiated animals. Depicted signals are bipolar derivations of fronto-parietal supra-dural electrodes (Surface EEG) and of depth electrodes located in the S1Cx, MoCx and VLTN. **(C)** Normalized power of EEG and LFP signals in the time-frequency plane corresponding to the seizures displayed in **(B)**. Baseline was the 2 s preceding seizure onset. Color code represents power-ratio between seizure and baseline.

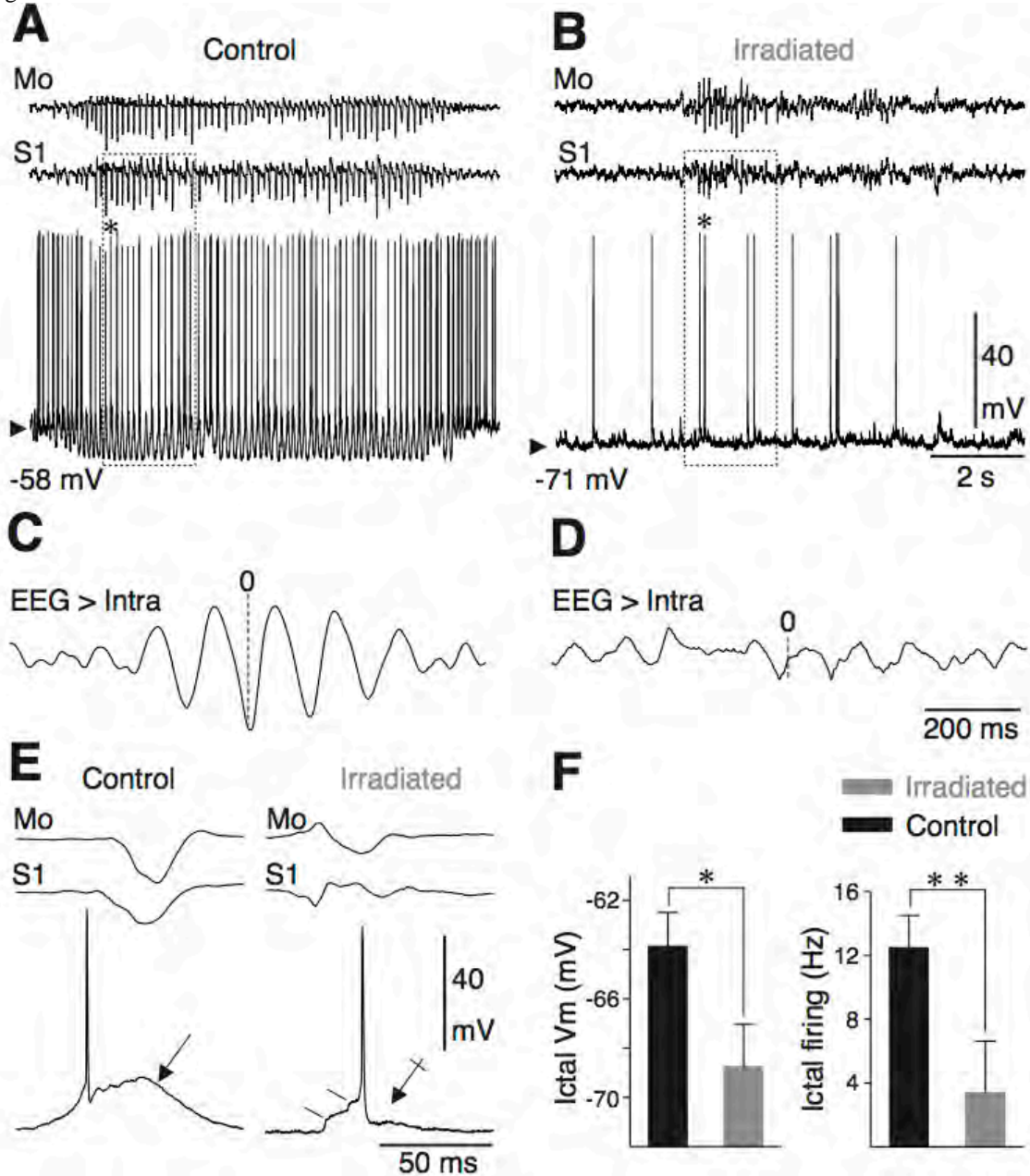
Figure 3.



Interictal activity of irradiated cortical neurons. **(A-B)** Interictal cortical LFPs of the S1Cx and corresponding intracellular activities (bottom records) from non-irradiated (A) and S1Cx-irradiated GAERS (B). Note the membrane hyperpolarization, the attenuation of background synaptic activities and the absence of spontaneous firing in the irradiated neuron. The left *inset* in (B) is an expansion of the dashed box. The right *inset* represents the MR image of the IntMRT targeted region at -1.4mm from bregma. The lowest white point indicates the location of the irradiated cortical

cell illustrated in (B) and (E). S1HL/FL: S1Cx hind-forelimb region; S1BF: barrel fields; CPu: caudate-putamen. (C) Membrane potential distributions (1 mV bin size,) calculated from 10 s subthreshold spontaneous activities in the non-irradiated and irradiated neurons shown in (A) and (B), respectively. The inset represents the standard deviation (SD) of background synaptic activities in control ($n = 19$) and irradiated ($n = 8$) neurons. (D-E) Voltage responses to ± 0.4 nA current pulses from the non-irradiated (D) and irradiated (E) neurons shown in (A) and (B), respectively. The *inset* in (E) shows the onset of voltage responses to -0.4 nA pulses. The inset in (D) is the superimposition of averaged action potentials ($n = 5-10$) from the non-irradiated (A) and irradiated (B) neurons. Note the constancy of action potential amplitude, kinetics and voltage threshold (dashed line). (F-G) Mean ($n = 20$) voltage changes (ΔV_m) as a function of the current intensity (I), from a non-irradiated (F) and irradiated (G) neuron. The apparent input resistance (R_m) was calculated from the ΔV_m-I curve. The dashed line in (G) is the linear fit computed in (F). (H) Values of membrane potential (V_m), spontaneous interictal firing rate, R_m and time constant (τ_m) in non-irradiated ($n = 19$) and irradiated ($n = 8$) neurons. * $P < 0.05$, ** $P < 0.001$, *** $P < 0.0001$.

Figure 4.



Intracellular activity of irradiated neurons during RPOs. (A-B) Intracellular activity (lower traces) of S1Cx neurons simultaneously recorded with the corresponding somatosensory and motor cortical LFPs during a SWD in a non-irradiated GAERS (A) and during RPO in a bilaterally-irradiated GAERS (B). The value of membrane potential is indicated at the left of the traces. (C-D) Crosscorrelograms between EEG and intracellular activities from the recording epochs, in the non-irradiated (C) and irradiated (D) GAERS. (E) Suprathreshold depolarizations (bottom records) recorded from non-irradiated and irradiated S1Cx neurons and the corresponding S1Cx and MoCx EEG paroxysms. Whereas the firing of the non-irradiated cortical neuron is generated by a smooth and prolonged, depolarization (oblique arrow), action potential discharge in the irradiated neuron is triggered by the temporal summation of discrete synaptic depolarizations (oblique lines) and followed by a lasting after-hyperpolarization (crossed arrow). (F) Values of membrane potential (Ictal Vm) and firing rate (Ictal firing), calculated during paroxysmal oscillations, in non-irradiated ($n = 19$) and irradiated ($n = 8$) S1Cx neurons. The location of the irradiated cortical cell illustrated in (B), (D) and (E) is indicated by the upper white point in Fig 4B (*inset*). * $P < 0.05$, ** $P < 0.001$.

Supplementary figure legends

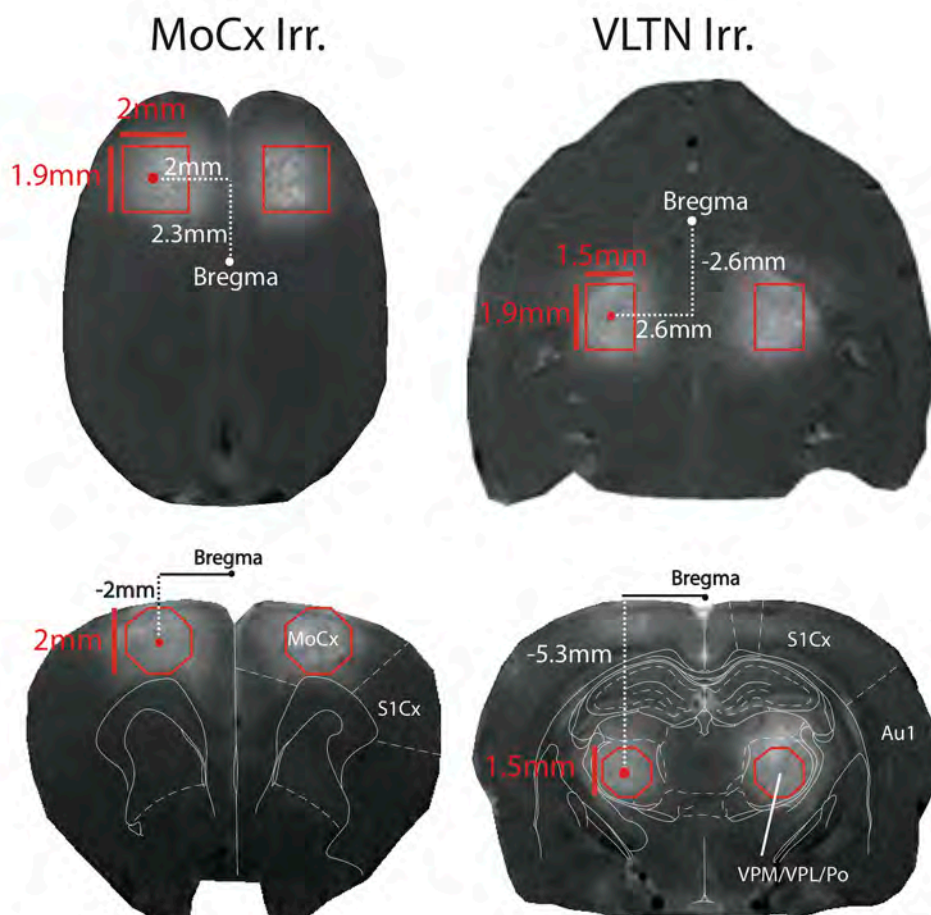


Figure S1 Theoretical delimitation (red lines) of IntMRT-irradiated volumes superimposed on horizontal (upper panel)

and coronal (lower panel) MR images acquired 14 days post-irradiation. Homogeneous dose deliveries (200 Gy) in the MoCx (left panels) and the VLTN (right panels) are obtained by interlacing arrays of 10 microbeams. CPU: caudate putamen (striatum); Au1: primary auditory cortex; VPM: ventral posteromedial thalamic nucleus; VPL: ventral posterolateral thalamic nucleus; Po: posterior thalamic nuclear group.

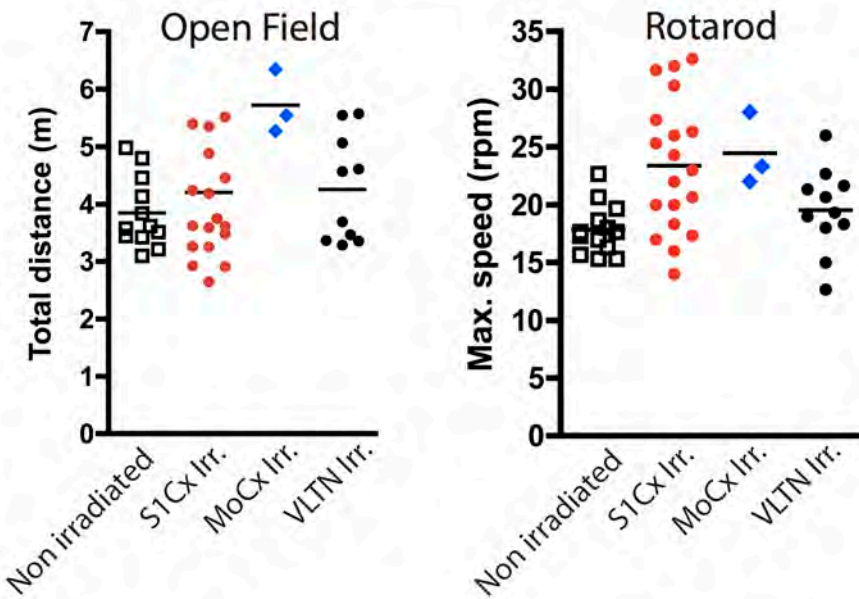


Figure S2 Assessment of post-irradiation sensory-motor behavior. Total distance travelled over 20 min in a 50 x 50 cm open field arena (upper panel) and 3-trial average of the maximum speed reached on the Rotarod® test. Each dot corresponds to one animal.

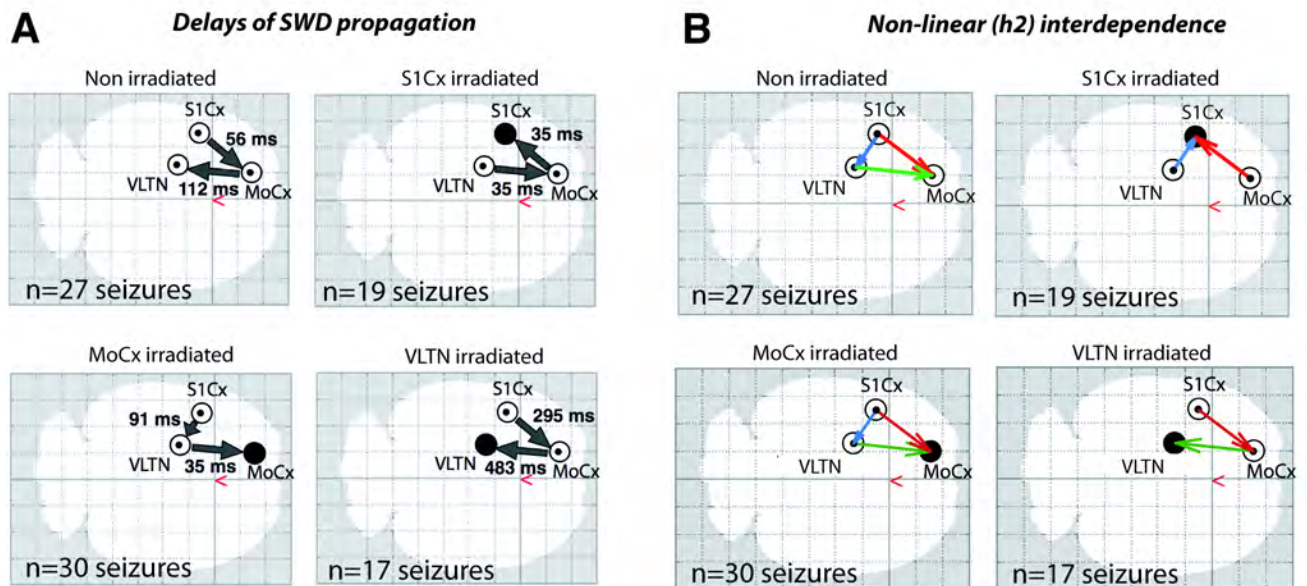


Figure S3 (A) IntMRT changed the sequence of SWD propagation in the three implanted brain areas. While in non-

irradiated animals, SWDs consistently started in the S1Cx, RPOs recorded in the irradiated volumes consistently lagged behind the two non-irradiated structures. SWDs always appeared first in the S1Cx in animals irradiated in the MoCx or the VLTN. By contrast, in S1Cx-irradiated rats, SWDs were first recorded in the VLTN, then in the MoCx. **(B)** Direction of dependence between EEG signals recorded from the different electrodes, as determined by non-linear association values (h^2) between pairs of electrodes during the first two seconds of seizures ($n = 17-30$). Arrows originate from the so-called driver. In non-irradiated GAERS, the S1Cx cortex drove both the MoCx and the VLTN, while in the other experimental groups the irradiated brain volumes were always driven by the other structures.

Movie S1. Screen capture of the progress of the bilateral irradiation of a GAERS's somatosensory cortex. At each step of the irradiation process, a diagram depicting the orientation of the microbeam array is showed. Speed is accelerated 8 times.